Research Journal of Applied Sciences, Engineering and Technology 3(1): 46-52, 2011
ISSN: 2040-7467

Received: November 25, 2010 Accepted: December 18, 2010 Published: January 20, 2011

Petrophysical Properties of North Sea Shales

K.S. Okiongbo
Department of Geology and Physics, Niger Delta University, Wilberforce Island, Bayelsa State

Abstract: This study presents a data set comprising estimated permeabilities of 22 natural mudstones which also have been characterised in terms of their pore size distribution, porosity, grain density and Total Organic Carbon (TOC) content. Pore size distribution and grain density were determined using mercury porosimetry and pycnometer method. TOC was determined by direct combustion of the organic carbon in LECO RLS-100 Carbon Sulphur analyser. Permeabilities were estimated based on the measured pore throat size distribution plus assumed pore alignment and pore shape using the model of Yang and Aplin. TOC and grain density ranges from 3.44- 9.98% and 2.61-2.70 g/cm^3, respectively. Porosity decreases from ~24-3% between the depth range of 1515-4781 m. The pore size distribution data show that the mean pore radius decreases from ~36-2 nm within the same depth range, the shift to smaller mean pore radii is driven primarily by the collapse of pores larger than 10nm with increase in consolidation. These values represent some of the smallest pore sizes known for rocks and in part provide a qualitative explanation for the low shale permeabilities. Estimated vertical permeabilities range from 9.5×10^{-23} to 8.6×10^{-21} m^2. In general, permeability decreases logarithmically with porosity.

Key words: Grain density, permeability, porosity, pore-size distribution, shales, total organic carbon

INTRODUCTION

Permeability measures the ease with which fluid flows through a porous medium and is the coefficient k in Darcy's law:

$$q = kA\ (\Delta h/L) \quad (1)$$

where,
q = flow rate (units of L^3/T); k = coefficient of permeability or hydraulic conductivity (L/T); A = cross sectional area (L^2); L = Length along flow path (L) and Δh = fluid head (pressure) loss along the flow path. $\Delta h/L$ is the hydraulic gradient I and is dimensionless.

The quantification of permeability underpins any understanding of fluid flow, both petroleum and water, in sedimentary basins. At the basin scale, mudstones are of particular importance due to their great abundance and low permeability. For example, low permeability inhibit consolidation and can thus lead to the development of overpressure both within the mudstones and within any more permeable units encased within them. Equally, mudstones inhibit the flow of petroleum toward the basin surface, with obvious economic implications. In many applications, such as the modelling of fluid flow in compacting sedimentary basins (Hermanrud, 1993; Schneider *et al*., 1993; Dewhurst *et al*., 1999) and the evaluation of basin slope stability (Dugan and Flemings, 2000), the relationship between permeability and porosity is required as one of the key constitutive equations.

However, because of the limited number of published mudstone permeabilities, there is very little quantitative understanding of permeability variation at either the microscopic or macroscopic scale (Yang and Aplin, 1998). Perhaps the main reason for the lack of permeability data is the difficulty of measuring the sub micro Darcy values which characterise mudstones, with porosities below thirty percent (Neuzil, 1994). Permeability is thus commonly estimated from more easily determined physical properties of mudstones such as porosity, pore size distribution or specific surface area (Leonards, 1962; Lapierre *et al*., 1990). Pore size data are especially useful in petroleum systems, not only because they can be used to infer permeability but because they are required for the assessment of capillary entry pressures and thus seal capacity and failure.

This study presents permeability, pore size distribution, and other physical data for 22 mudstone samples from the North Sea basin and the Norwegian Margin. The samples were carefully chosen so that we could investigate the influence of consolidation on pore size distribution and permeability of mudstones.

Geological setting: The Northern North Sea is the area North of 55ºN (the Mid North Sea high) to about 62ºN,

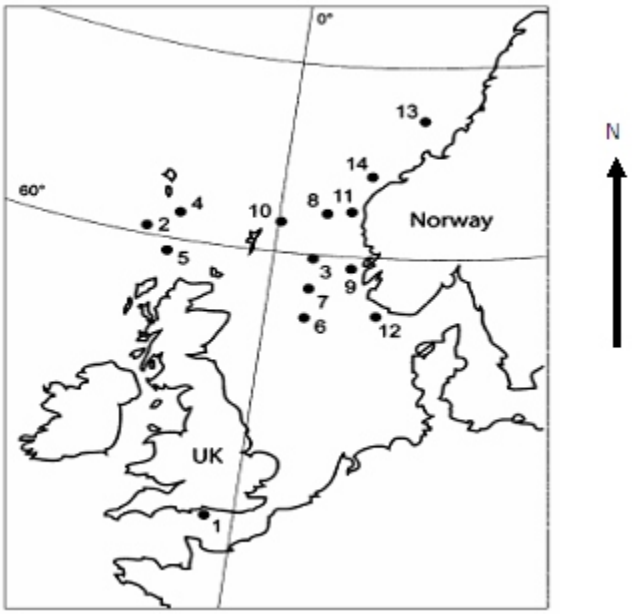

Fig. 1. Map of the study area showing well locations

and includes all basins within the area both in the UK and Norwegian sectors of the North Sea (Fig. 1). Its geological evolution has been extensively discussed in various papers (Nielsen *et al*., 1986; Thorne and Watts, 1989). The North Sea is a Paleozoic to Holocene multistage rift basin within the north western European cratonic block. It is superimposed on the Caledonian Orogenic trend. The tectonic framework of the northern North Sea consists of a north-trending Viking Graben, which intersects in the South, the South easterly-orientated Central Graben and the westerly Witch Ground Graben.

The lithologies are composed of sands and shales in the Triassic - Jurassic section of the basin and locally organic matter (e.g., Kimmeridge Clay) is present. In the Cretaceous, the lithologies are dominantly carbonates and shales. They are mainly shales, silts and sands in the Tertiary with an interruption in the Paleocene when Volcanism occurred. This corresponds to the widespread deposits of volcanic tuffs all over the graben (Hancock, 1990).

MATERIALS AND METHODS

Twenty-two core samples were selected from 16 wells from the northern parts of the North Sea and the Norwegian Margin. The main sampling criterion was sample quality, since high quality core materials is a prerequisite for the accurate determination of very low permeabilities. Standard techniques were employed to evaluate grain density (the small pycnometer method at 20ºC) and Total Organic Carbon (TOC) by direct combustion of the organic carbon in LECO RLS-100 Carbon Sulphur analyser. Approximately 5-10 g fragments were cut from the 22 mudstone core samples. Samples were dried first at room temperature and then for 24 h at 105ºC. There was no visible alteration of sample integrity resulting from the cutting or drying procedure.

Pore-size distribution of the mudstone specimens was determined by mercury intrusion porosimetry, following the procedure described by Issler and Katsube, (1994). In principle, the mercury porosimeter can generate pressures high enough to force mercury into all accessible pores and measure the volume of mercury taken up by them (Rootare, 1970). Assuming cylindrical pore shapes, the Washburn equation (Rootare, 1970) relates the amount of pressure, p, required to force mercury into pores with pore-size diameter, d, greater than or equal to:

$$d = -4\gamma\cos\theta / p \quad (2)$$

where, γ is the surface tension of mercury, and θ is the contact angle. Values of $\theta = 141^{\circ}$ and $\gamma = 0.48$ N/m were used in this study. The measurements were made using a Micrometrics Autopore II 9220 mercury porosimeter with an available pressure range of 0.021-269 MPa and an equivalent pore-size range of 3-36444 nm.

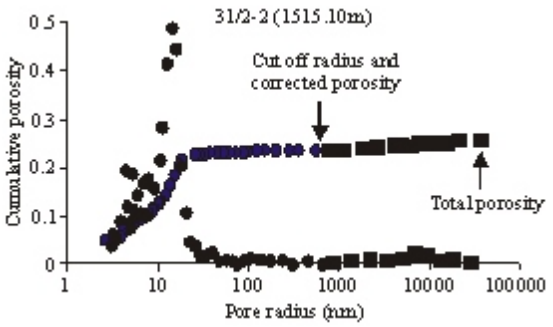

Fig. 2: Example of pore-size distribution, the blue plot marks the cumulative porosity against pore size distribution. The red plot marks the pore density against the pore size distribution

The mercury injection pressure was incrementally increased from 0.021 to 269 MPa in 56 pressure steps, and the volume of mercury intruded for each step measured. Knowing both the applied pressure and the incremental volume of mercury intruded into the sample allows pore-size distributions throughout the sample to be calculated from Eq. (2). The total porosity was calculated from the dry bulk density and the measured grain density. The dry bulk density was calculated from dry weight and bulk volume given by the mercury intrusion. Since sampling and unloading may induce some microfracturing, the total porosity was corrected using pore size distribution data. The approach, illustrated in Fig. 2, is to determine the point at which the pore size frequency curve, when plotted as a function of increasing pore radius becomes a minimum. It is assumed that pores above that "cutoff" radius are sampling artefacts and are removed from the data set.

The mean pore throat radius was calculated for all pores smaller than the cut off radius. It was calculated incrementally from the relative pore size distribution using the equation (Yang and Aplin, 2007).

$$\bar{r} = \sum_{i} \left(\phi_{\%,j} - \phi_{\%,j-1} \right) \exp\left(\frac{\ln(r_{i-1}) + \ln(r_i)}{2} \right) \quad (3)$$

where, r_i is the pore throat radius at data point i(nm), ϕ%, i is the fractional relative porosity at pore throat radius r_i and is defined as:

$$\phi_{\%,j} = \phi_{cum,j} / \phi_c \quad (4)$$

where, $\phi_{cum,i}$ is the fractional cumulative porosity at data points i and ϕ_c is the corrected porosity. In the calculation of mean pore throat radius using above equations, pores smaller than the smallest measured pore (3.0 nm in this work) were neglected since their contribution to the mean pore throat radius is insignificant.

Permeability was modelled from the pore throat size distribution and porosity data using the approach of Yang and Aplin, (1998). Yang and Aplin permeability model is based on the pore throat size distribution, an assumed pore shape comprising two frustra of cones connected at their base and an alignment angle of pores. Both the pore shape and alignment change with increasing compression, developing a higher aspect ratio and becoming increasingly perpendicular to the direction of maximum compressive stress. Yang and Aplin permeability model is based on the following equations:

Vertical permeability:

$$K_v = 10^{-19.21} J_v^{1.118} r^{-1.074} \quad (5)$$

Horizontal permeability:

$$K_h = (\text{ctan}(\alpha))^{2.236} K_v \quad (6)$$

where,

$$J_v = 9/8\ \phi\ (\sin(\alpha))^2\ (J_1^3 / (1 + J_1 + J_1^2)^2) \quad (7)$$

$$J_1 = 2.371 - 1.62\text{clay}^2 + 153.8\ \phi^4 \quad (8)$$

$$\alpha = 45^o - 10.24^o\ (e_{100} - e) \qquad \sigma^1 > 100\text{kPa}$$
$$\alpha = 45^o \qquad \sigma^1 > 100\text{kPa} \quad (9)$$

$$e_{100} = 0.3024 + 1.687\text{clay} + 1.951\text{clay}^2 \quad (10)$$

K_v and K_h are absolute vertical and horizontal permeabilities (m^2), $\bar{r}$ is the mean pore throat radius (nm), ϕ is porosity, e is void ratio = ϕ / (1-ϕ), e_{100}, is void ratio at 0.1 MPa effective stress, J_1 is the ratio of the largest radius of a pore to its throat radius, assumed to be the same for all pores for a given sample, α is the average pore alignment angle relative to bedding direction (degree), clay is the fractional clay content, and σ^1 is effective stress. Inputs for the Yang and Aplin permeability model are thus porosity, pore size distribution and clay content. From these inputs, J_1 and α are calculated from clay content and porosity using Eq. (8), (9) and (10), respectively, and $\bar{r}$ from the pore size distribution using Eq. (3).

Table 1: Summary of petrophysical properties and modelled permeabilities

S.No.	Well no.	Depth (m)	TOC (%)	Grain density (gcm^3)	Porosity	Mean radius (nm)	Permeability (nD)
1	31/2 - 2	1515	4.16	2.69	0.242	13.5	4.800
2	35/11 - 4	1979	4.03	2.69	0.095	14.3	1.400
3	31/4 -10	2007	5.91	2.67	0.110	7.8	0.870
4	31/4 - 9	2117	9.53	2.61	0.205	6.1	1.600
5	31/4 - 6	2132	7.05	2.64	0.192	6.3	1.500
6	34/10 -18	2352	5.61	2.67	0.164	34.5	7.300
7	30/9 - 10	2755	3.69	2.70	0.165	35.6	8.600
8	30/9 - 14	2978	3.06	2.86	0.103	6.3	0.640
9	211/12A - M1	3125	8.21	2.64	0.143	13.0	2.100
10	211/12A - M1	3282	5.81	2.63	0.152	12.7	2.300
11	211/12A - M16	3376	9.77	2.65	0.243	10.9	3.800
12	211/12A - M16	3401	8.18	2.69	0.238	15.7	5.500
13	34/8 - 6	3578	9.43	2.61	0.128	2.3	0.290
14	16/7b - 20	3932	7.53	2.63	0.093	1.2	0.095
15	16/7b - 20	4030	7.42	2.65	0.105	2.2	0.081
16	16/7b - 28	4120	8.34	2.64	0.072	2.9	0.180
17	16/7b - 20	4134	11.10	2.62	0.080	3.8	0.270
18	16/7b - 20	4158	5.85	2.62	0.052	2.5	0.100
19	3/29 - 2	4608	6.91	2.67	0.064	3.2	0.170
20	3/29a - 4	4707	4.46	2.68	0.043	2.0	0.067
21	3/29a - 4	4742	6.37	2.67	0.048	2.5	0.095
22	3/29a - 4	4781	6.16	2.66	0.033	4.3	0.100

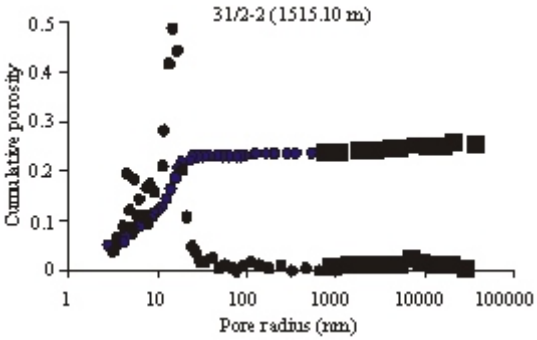

(a)

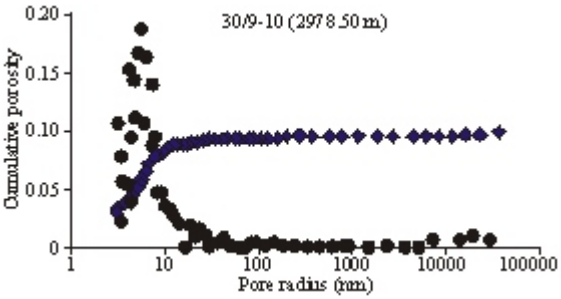

(c)

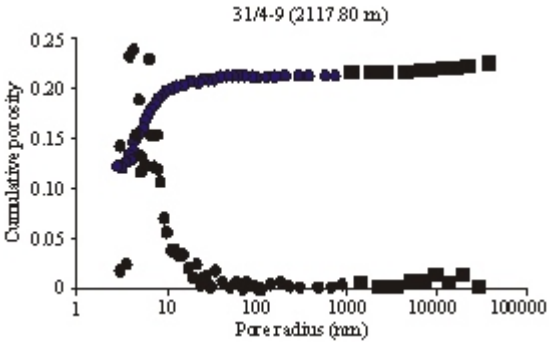

(b)

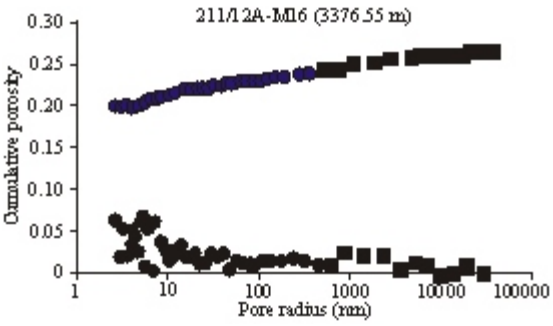

(d)

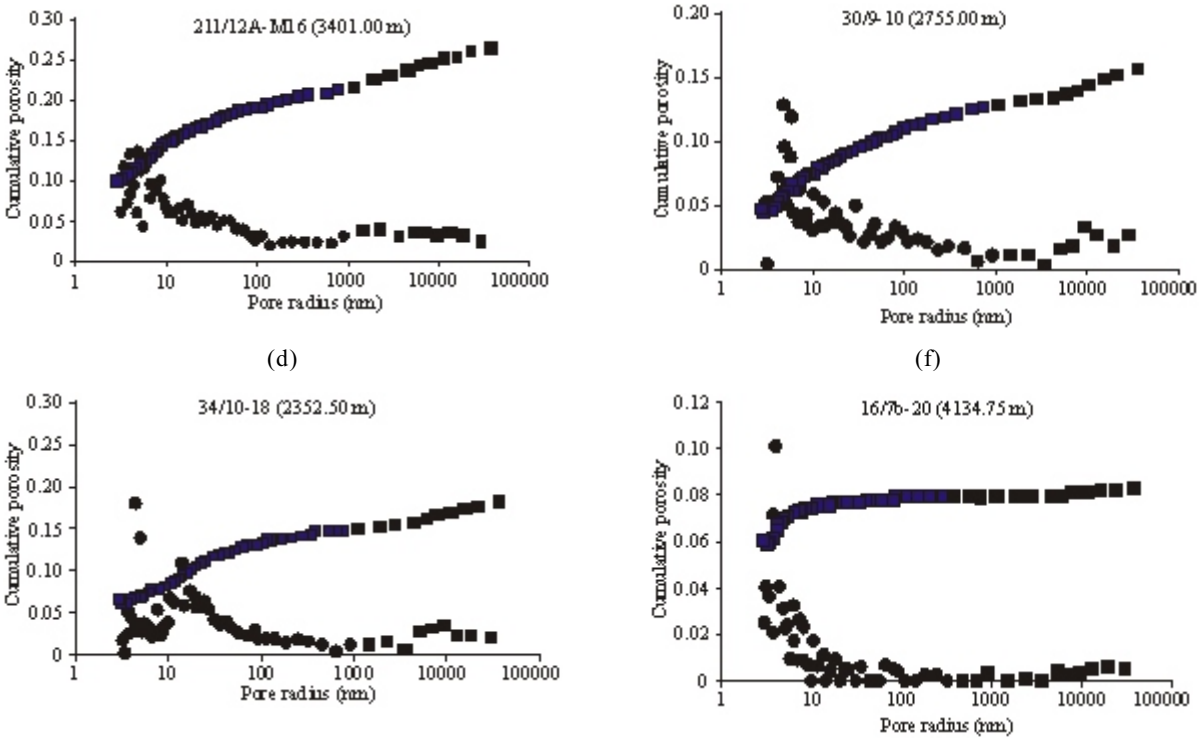

Fig. 3: Measured pore-size distributions

RESULTS AND DISCUSSION

The data set is presented in Table 1, with pore throat size distribution data shown in Fig. 3. Pore throat sizes and porosity range from ~3.0-1000 nm and ~3.0-24% respectively. Figure 3 shows that the mudstones are characterised by unimodal pore size distributions with modes decreasing from ~15 nm at 1515 m to ~6-8 nm as depth increases to 4781 m. Generally, the sample suite is characterised by larger porosities and pore sizes at shallow depth but decreases from ~15 nm at about 24% (1515 m) to ~1.2-5.0 nm at porosities <10% suggesting that with increasing effective stress, porosity is lost by the collapse of relatively larger pores, resulting in a decrease in the mean pore throat size (Yang and Aplin, 1998). Figure 4 shows that mean pore radius is almost constant at values <5.0 nm suggesting a state of maximum compaction as the porosity approach a critical value of <10%. This reaffirms the fact that most of the porosity loss occurs through the collapse of pores larger than 10 nm (Yang and Aplin, 1998). A lower limit of ~3.0 nm pore radius was determined at a pressure of 269MPa in all samples. Since mudstones contain pores with radii smaller than 3.0 nm and/or have pores which are not connected to the flow system, the pore size distributions do not start at zero porosity but a porosity which represents difference between the total porosity and that measured by mercury intrusion.

Close examination of Fig. 3 reveals two pore size distribution patterns. One typified by Fig. 3a and has scarcely any pore throats above 100 nm (no significant penetration at radii >100 nm) and mean pore radii are not more than 14.0 nm. The other, Fig. 3d has much broader pore size distribution pattern with pores up to 10^3 nm in radius maintained to depth levels in excess of 2500 m. Samples 1-5, 8 and 13-22 fall in the first category (group A), numbers 6, 7, and 9-12 in the second category (group B). Samples in group B have higher porosity, broad pore size and mean pore radius which is almost two orders of magnitude greater than that of samples in group A.

Permeabilities calculated using Eq. (4) are plotted against depth in Fig. 5 and against porosity in Fig. 6. Calculated permeabilities range between 9.5×10^{-23} - 8.6×10^{-21} m^2 (8.6-0.095 nD). This range is within that reported by Neuzil (1994) for permeabilities determined

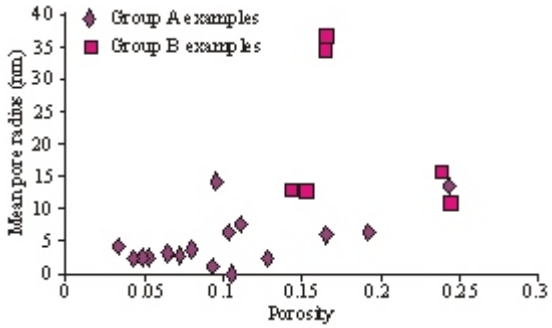

Fig. 4: Mean pore radius as a function of porosity

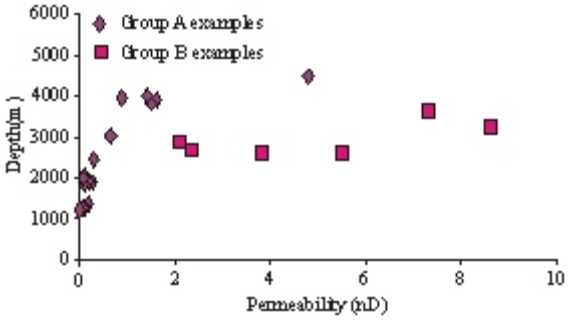

Fig. 5: Permeability as a function of depth

both experimentally and inferred for field settings by inverse analysis of pressure or flow data. Figure 5 shows an overall decrease in permeability from 8.6×10^{-21} m^2 (8.6nD) to 9.5×10^{-23} m^2 (0.095 nD) at a depth and porosity range of 1515-4781 m and 3.0-24%, respectively, a decrease of about three orders of magnitude. The two distinct permeability-depth trends observed in Fig. 5 reflects the pore size distribution patterns earlier mentioned above and demonstrates the key importance of pore size distribution as a control on permeability (Dewhurst *et al*., 1998). In group A samples, permeability decreased in an exponential fashion from ~9.5×10^{-23} to 4.8×10^{-21} m^2 within the depth range of 1515-4781 m as the porosity changes from ~24-3.3%. The trend defined by samples in group B is rather linear (Fig. 5). In this group, permeability decreased from ~2.1×10^{-21} to 8.6×10^{-21} m^2 within the depth range of 2755-3401m as porosity changes from ~24-15%. There is some evidence that samples in this group have a slightly higher permeability values than samples in group A at a given porosity (Table 1). In general, at higher porosities, coarser grained mudstones have higher permeabilities than finer grained mudstones, reflecting their greater mean and maximum pore throat sizes (Yang and Aplin, 2007). There is a variation of about two orders of

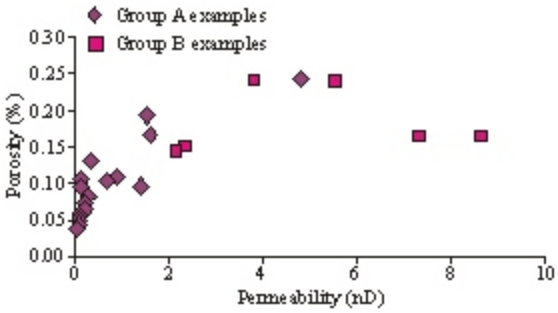

Fig. 6. Porosity -permeability relationship

magnitude in permeability at a given porosity at porosities >10% with a decreasing range as porosity decreases, converging at a porosity and permeability of ~0.13 and <2.0×10^{-21} m^2, respectively (Fig. 6). Since lithology (clay content) exerts a key control on pore size distribution, much of the variation of permeability observed at a single porosity according to Yang and Aplin, (2007) can be explained by lithological differences.

CONCLUSION

Twenty-two cored mudstone samples are characterised in terms of their pore size distribution, porosity, grain density and total organic carbon. Permeabilities were estimated based on the measured pore throat size distribution plus assumed pore alignment and pore shape. The results show that the shales displayed extremely small pores, mainly concentrated in the 0.3-60 nm range, in the form of a unimodal distribution. These values represent some of the smallest pore sizes known for rocks. In addition, the modes (3-12 nm) of these distributions appeared to represent the pore sizes of the main fluid-flow paths of these shales, thus providing a qualitative explanation for the low shale permeabilities. Porosity and vertical permeability range between 3.3-24% and 9.5×10^{-23} - 8.6×10^{-21} m^2, respectively. In general, permeability decreases logarithmically with porosity. Permeability is a function of porosity and lithology.

ACKNOWLEDGMENT

I am grateful to A.C. Aplin and Steve Larter for the guidance during my research at Newcastle Upon Tyne. I also wish to thank my surrogate parents in England, Mr and Mrs Peter Nicolls for the financial support during my stay in Newcastle Upon Tyne.

REFERENCES

Dewhurst, D.N., A.C. Aplin, J.P. Sarda and Y. Yang, 1998. Compaction-driven evolution of porosity and permeability in natural Mudstones: an experimental study. J. Geophys. Res., 103(B1): 651-661.

Dewhurst, D.N., Y. Yang and and A.C. Aplin, 1999. Permeability and Fluid Flow in Natural Mudstones. In: A.C. Aplin, A.J. Fleet and J.H.S. Macquacker (Eds.), Muds and Mudstones: Physical and Fluid Flow Properties. Geological Society, London, Special Publications, 158: 23-43.

Dugan, B. and P.B. Fleming, 2000. Overpressure and fluid flow in the New Jersey Continental Slope: Implications for slope stability failure and cold seeps. Science, 289: 288-291.

Hancock, J.M., 1990. The Cretaceous. In: Glennie, K.W. (Eds.), Introduction to the Petroleum Geology of the North Sea. Blackwell Scientific Publications, pp: 255-272.

Hermanrud, C., 1993. Basin Modelling Techniques - An Overview. In: Dore, A.G. (Ed.), Basin modelling Advances and Applications. Norwegian Petroleum Society Special Publication 3, Elsevier, New York, pp: 1-34.

Issler, D.R. and T.J. Katsube, 1994. Effective porosity of shale samples from the Beaufort-Mackenzie Basin, Northern Canada. In Current Research, 1994-B, Geological Survey of Canada, pp: 19-26.

Lapierre, C., S. Leroueil and J. Locat, 1990. Mercury intrusion and permeability of Louiseville clay. Can. Geotech. J., 27: 761-773.

Leonards, G., 1962. Engineering Properties of Soils. McGraw-Hill, New York.

Neuzil, C.E., 1994. How permeable are clays and shales? Water Resour. Res., 30: 145-150.

Nielsen, O.B., S.S. Sorensen, J. Thiede and O. Skarbo, 1986. Cenozoic differential subsidence of the North Sea. AAPG, 70: 276-298.

Rootare, H.M., 1970. A review of mercury porosimetry. Perspect. Powder Metall., 5: 225-252.

Schneider, F., J. Burrus and S. Wolf, 1993. Modelling Overpressures by Effective Stress/porosity Relationships in Low-permeability Rocks: Empirical Artifice of Physical Reality? In: Dore, A.G. (Ed.), Basin Modelling; Advances and Applications, Norwegian Petroleum Society, Special Publication 3, Elsevier, New York, pp: 333-341.

Thorne, J.A. and A.B. Watts, 1989. Quantitative analysis of North sea subsidence. AAPG, 73: 88-116.

Yang, Y. and A.C. Aplin, 1998. Influence of lithology and compaction on the pore size distribution and modelled permeability of some mudstones from the Norwegian margin. Mar. Petrol. Geol., 15: 163-175.

Yang, Y. and A.C. Aplin, 2007. Permeability and petrophysical properties of 30 natural Mudstones. J. Geophys. Res., 112: 1-14.